

# Shallow diffraction imaging in an SH-wave crosshole configuration

Ariel Lellouch<sup>1</sup> and Moshe Reshef<sup>1</sup>

## ABSTRACT

Imaging shallow subsurface voids, such as karsts, sinkholes, pinch-outs, dikes, and man-made voids, is an important task in near-surface geophysics. We have developed a new diffraction-based methodology for void detection and imaging. Due to the low signal-to-noise ratio of the diffracted signal in surface acquisition setups, we advocate the use of an SH-wave multicomponent crosshole acquisition. Naturally, the same setup can be used for velocity model building using tomography and for void imaging. The SH-wave data are migrated using a model-based, image-point-dependent automatic muting function that separates direct arrivals from diffracted events in the migration process. For the purpose of location and velocity analysis, data are migrated to the depth imaging offset domain. Only when the velocity model and imaging locations are correct will the diffracted energy be coherently focused to the void location and the diffracted event moveout in the migrated gather will be flat. We found that the received diffracted signal is clearer and has better temporal separation compared with a conventional P-wave crosshole survey. We determined the usefulness of this method using synthetic and field data examples for 2D acquisitions and a synthetic 3D case, showing that a precise imaging is possible. The importance of the S-waves velocity model, which can be extracted from the same survey using conventional tomography methods, is also discussed.

## INTRODUCTION

Accurately detecting and localizing subsurface elements of a diffractive nature, such as karsts, sinkholes, pinch-outs, dikes, and man-made voids is an important task in shallow seismic exploration (Walters et al., 2007; Peterie et al., 2009; Sloan et al., 2012). Several geophysical methods, such as microgravity (Rybakov et al., 2001),

electromagnetics (Auken et al., 2006), ground-penetrating radar (Cassidy et al., 2011), and seismic, have been tried, yielding the conclusion that seismic waves penetrate further and with higher resolution than any other potential geophysical method (Belfer et al., 1998). However, the use of seismic waves in the shallow subsection might be challenging due to its high complexity, poor data quality, and limited acquisition setup.

Seismic diffraction imaging is important in near-surface and exploration geophysics (Berkovitch et al., 2009). Due to the complexity of the seismic wavefield, containing a multitude of events, separation of the diffracted part of the signal is a necessary step prior to imaging (Fomel et al., 2007; Landa et al., 2008). Once the separation has been conducted, diffracted data can be used for imaging in a relatively straightforward manner. However, despite the fact that many migration operators are implemented using the virtual diffraction assumption (e.g., Kirchhoff), the imaging condition needs to be modified to match real diffractions instead of reflections (Khaidukov et al., 2004).

Following exploration seismic surveys, most attempts at tackling this problem have been made using surface-only surveys. Despite the obvious acquisition simplicity, data are affected by surface wave interference, cultural noise, and near-surface effects. This situation is worsened by the weak diffraction signal compared with direct, reflected, and refracted waves (Landa and Keydar, 1998), which turn it unusable for imaging. Therefore, considerable effort is required to separate the diffracted signal from the total seismic wavefield before imaging.

A costlier alternative is using downhole methods, which have been shown to be useful for a variety of applications (e.g., for a detailed overview, see Dietrich and Tronicke, 2009). These methods can provide higher resolution, especially when they are used in crosshole setups (Paasche et al., 2013), and they have the advantage of the higher signal-to-noise ratio (S/N) of diffracted events (Shustak et al., 2015).

Furthermore, most studies focus exclusively on P-waves under the acoustic assumption, thus disregarding a significant and often larger part of diffracted energy in the form of later S-phases. However, several authors (Dasios et al., 1999; Korneev, 2009) recognize the advantages of using S-waves in shallow subsurface surveys.

Manuscript received by the Editor 24 March 2016; revised manuscript received 7 August 2016; published online 7 November 2016.

<sup>1</sup>Tel Aviv University, Department of Earth Sciences, Tel Aviv, Israel. E-mail: lellouch@gmail.com; moshe@luna.tau.ac.il.

© 2017 Society of Exploration Geophysicists. All rights reserved.

In the following, we suggest the use of a multicomponent crosshole-based acquisition setup, optimized for SH-wave usage. Such a setup has the benefits of a better S/N as well as clear separation between the diffracted and direct S-waves. The data are migrated using a standard Kirchhoff migration that includes an automatic, image-point-dependent and model-based mute, separating direct and diffracted events, that was developed for this study. It holds significant advantages over the trivial shot-gather muting because the automatically calculated muting function is different for every imaging point and is velocity model dependent.

### OPTIMAL ACQUISITION SETUP

An adequately planned acquisition setup can greatly simplify different processing and imaging steps and should thus be correctly designed. The field acquisition setup should be optimized for a few parameters. First, it has to maximize the separation in time between diffracted and direct/reflected waves. Without such a separation in the acquisition stage, considerable effort will be needed in extracting the diffracted part, which is of our interest, from the total seismic field. Such effort is not guaranteed to be fruitful because various seismic events might reach a given receiver at the same time and interfere with each other. Because diffractions are significantly weaker than other events, their recovery might be strongly hindered from this interference. Second, given the weak diffracted signal, it needs an as-high-as-possible S/N. Finally, from a practical point of view, the acquisition should be as simple as possible to implement.

Surface acquisition systems are limited by the S/N criterion. First, it is very sensitive to surface wave noise, whether induced by the source as an undesired side effect or cultural, because it can easily mask diffracted energy. Moreover, diffracted energy is usually one to two orders of magnitude smaller than reflected/direct waves' energy (Landa and Keydar, 1998). Recent seismic studies in the shallow subsurface (Shustak et al., 2015) show that using surface-only acquisition, diffraction detection and imaging are practically unfeasible. However, this is only true for the studied areas and is not always the case. Due to their ease of deployment, surface surveys may be complementary or even used as a reconnaissance tool to determine ideal borehole locations in other sites.

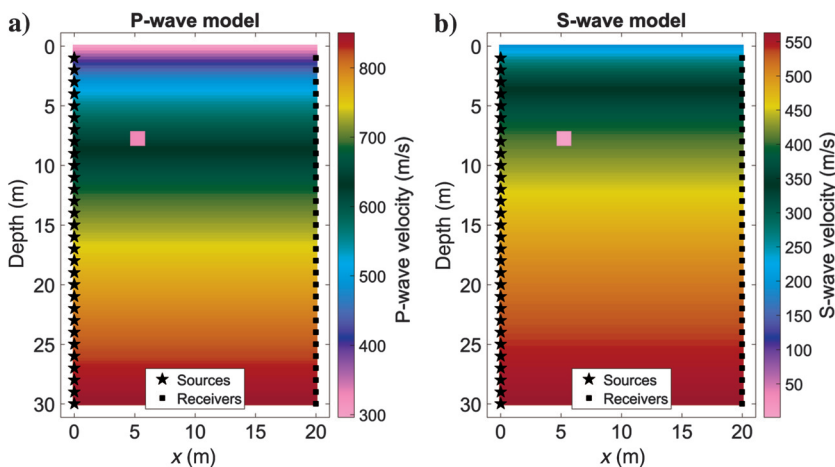


Figure 1. Simulative 2D crosshole setup across the narrow section of a long void with (a) P and (b) S velocity models. The void, filled with air, extends across the y-axis (outside of the drawn section plane).

In Figure 1, our suggested setup is presented. Using 3D forward modeling, a complete crosshole survey was generated. The survey is essentially in 2D, but it is computed in a 3D setup to allow for all possible waves to propagate. As shown in Figure 1, the survey area slices the narrow section of a long void, filled with air and extending across the y-dimension. The void's cross section is  $1.25 \times 1$  m. Source directivity remains an important issue as, in contrast to explosive ones, the field sources used in the later parts of this study were directional. Due to our borehole source operating mechanism, sources in the z-direction cannot be produced and will not, therefore, be presented.

If an SH-wave encounters a certain diffractive object, scattered waves will still be of an SH nature (Manoogian and Lee, 1996). For P- and SV-waves, in contrast, such discontinuities will cause mode conversions. Therefore, a correctly designed acquisition setup, whether on the surface or in a borehole, should theoretically contain SH events only. This is true because for the class of models we handle in this study, there are no clear reflective boundaries that could break the orthogonality between SH- and P/SV-waves nor signs of anisotropy. Because in the near surface, time differences between phases of arrivals are small (Lellouch and Reshef, 2016), decoupling the P/SV-waves from the seismic record may prove very beneficial. In Figure 2, one can see the difference in the recorded 3C signal due to source polarity. From this example, it is clear that using an SH-configuration, in which the source polarity and the receiver component are in the y-direction (perpendicular to the survey area), is optimal in terms of separation between direct and diffracted events. Any other combination yields a complicated mix of events in which diffractions are harder to separate, as expected from theory. Therefore, it seems that despite the operational difficulty, an SH crosshole setup will yield optimal data for diffraction imaging.

A remaining acquisition question is whether a full crosshole survey is required for a simulative setup, setting S/N problems aside. In other words, the data shown in Figure 2 could possibly be enough for imaging. Let us look at the full SH data from a crosshole survey as shown in Figure 3. This example shows us that despite the ideal simulative data, there are source depths at which we cannot separate direct events from diffracted events, and therefore, a diffraction-based imaging procedure is bound to fail. Thus, a full crosshole survey containing sources/receivers above and below the targeted void is needed for more than S/N practical reasons.

### DIFFRACTION SEPARATION AND IMAGING

In conventional diffraction imaging, an important task prior to imaging is the extraction of the diffractive component of the data. In those cases, the data contain mostly reflective events, and extensive studies have been conducted on separation methods. However, in the setup we advocate, there are no clear reflective events. On the contrary, both direct and diffracted arrivals, which we are trying to separate, are of a diffractive nature. Because there is no clear physical behavior difference between the two, separation is a much more challenging goal. Therefore, we advocate for a new separation method.

In Figure 3, we have seen the main problem of diffraction imaging in this setup — they are not always separated from direct arrivals. Imaging stronger direct arrivals would cause errors and possibly

turn the image unusable. Therefore, a separation of these events is needed. Nonetheless, due to very short time differences between the events (as shown in Figure 3) muting common-shot/receiver gathers, even manually, is practically impossible. However, as is common for any imaging task, we assume a known velocity model. This model could be used for an automatic model-based muting procedure. In this work, we use an eikonal-based Kirchhoff migration. For every image point, two types of traveltimes are calculated — to every source point  $t_S$  and to every receiver point  $t_R$ . Imaging consists of summing the matching trace sample at  $t_S + t_R$  to that image point. We propose applying an image-point-dependent muting scheme. Because the model is known, one can calculate the direct traveltimes  $t_D$  from each source point to all receivers using the same eikonal solver. Because we want to exclusively use diffracted events, the muting condition, calculated per image point, is that if and only if  $(t_S + t_R) - t_D > S$  will the relevant trace sample be summed into the specific image point. In this condition,  $S$  is a data-dependent separation parameter, usually taken to be about half a wavelet of the main frequency. In other words, if and only if the diffracted time is significantly separated from the direct traveltimes will the relevant trace data be taken into account. This muting scheme minimizes the inclusion of direct waves' energy during the migration at the cost of not migrating all available data. An example of the result of this procedure, proving its necessity, is shown in Figure 4.

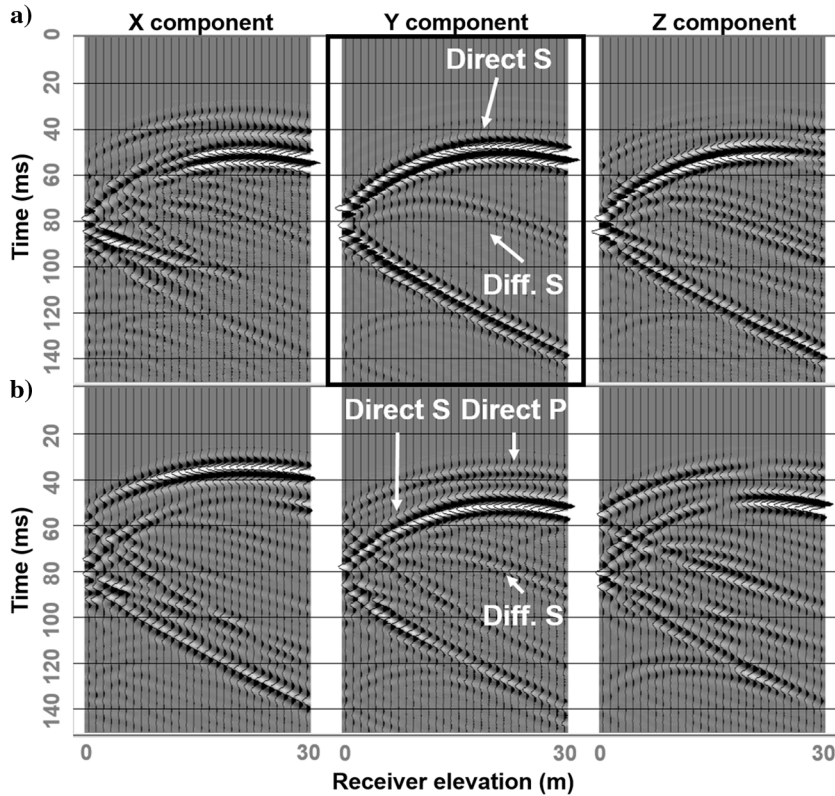


Figure 2. Three-component recorded signal from a source in the y-direction (a) and x-direction (b). Notice that the y-component recording a source in the same y-direction, or SH-configuration, yields a record containing only S-phases and with a clear distinction between direct and diffracted events.

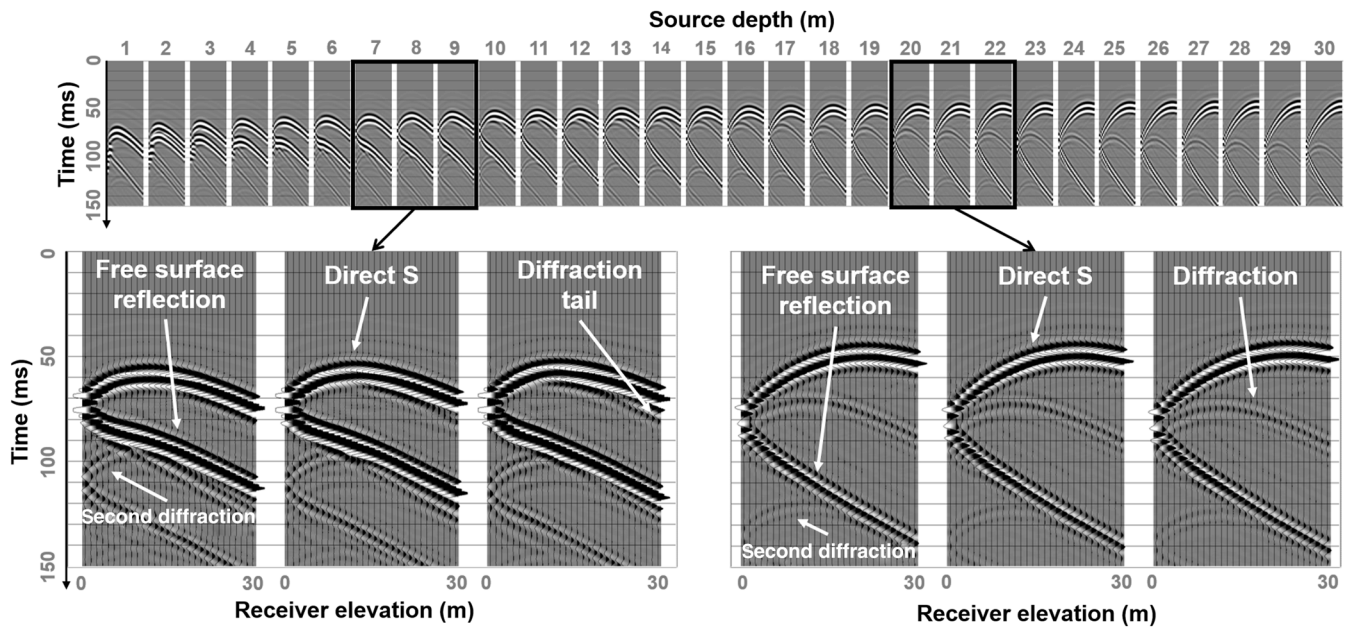


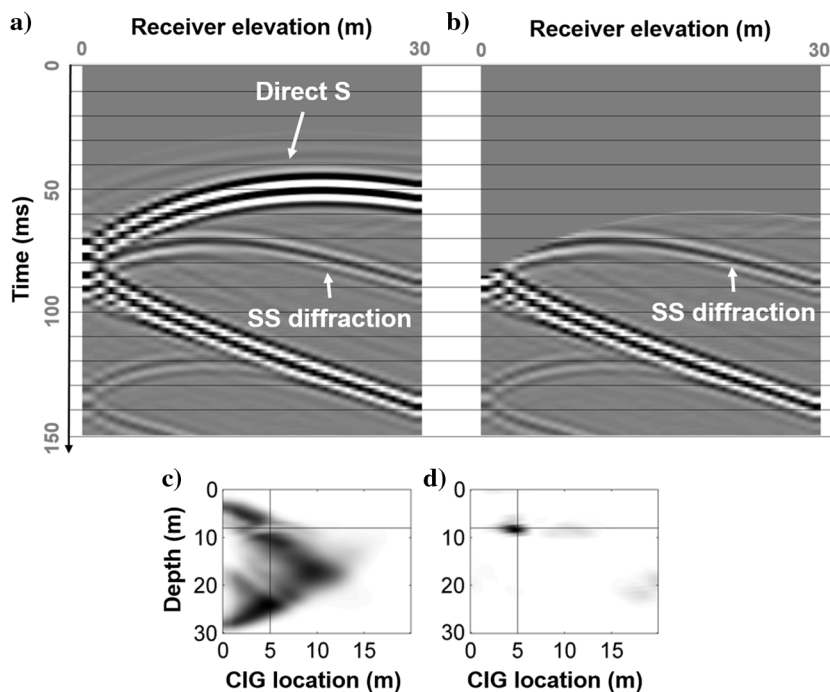
Figure 3. Full crosshole survey SH data. For certain source depths, there is a clear separation between direct and diffracted events, whereas for others, they cannot be differentiated.

Downloaded 11/09/16 to 79.177.51.113. Redistribution subject to SEG license or copyright; see Terms of Use at http://library.seg.org/

## DIFFRACTION-BASED COMMON-IMAGE GATHERS AND VELOCITY/LOCATION ANALYSIS

Instead of directly imaging the data, as shown in Figure 4, one can first migrate it into common-image gathers (CIGs), here using a standard Kirchhoff migration. Those gathers are extensively used for migration velocity analysis (MVA) procedures, and their flatness is indicative of a correct velocity model. In this study, however, the diffraction point is also unknown, and therefore it must also be estimated using the CIGs. Thus, we suggest using them for a joint location and velocity analysis with conventional MVA techniques. The nonconventional acquisition setup requires a suitable image domain. In this study, we follow the imaging offset concept (Biondi, 2006). As shown in previous studies (Reshef, 2001), imaging offset gathers offer a more effective way to control the velocity analysis procedure. Therefore, we rotate the entire problem by  $90^\circ$  and define the depth imaging offset, which is the depth of the receiver minus the depth of the image point, and we migrate the data to these gathers. In Figure 5, we show the CIGs for different imaging points, and in Figure 6, a velocity analysis at the correct location is shown. These examples show the high sensitivity of the depth imaging offset gathers to errors in the location and velocity models. Besides manual inspection, the flatness of the migrated events in the gathers can be automatically measured. In this study, we chose semblance as a flatness/coherence criterion instead of stacking because it is a more accurate measure of energy focusing on the diffraction location, assuming a given velocity model. For every CIG, we measure the semblance using a window matching the wavelet size of the data in depth. The result is a semblance trace varying with depth. This procedure needs to be repeated for every possible CIG within a reasonable resolution because we do not know the diffraction point location. Then, the different semblance traces are combined into a semblance image, whose dimensions are  $\{x \text{ location, depth}\}$ , and the value at each point in space is its measured semblance. If the correct velocity model is used, the semblance value is to

Figure 4. Imaging with and without direct wave muting. The correct location is denoted by the intersection. (Top) Mute effects at the correct imaging point — original (a) and muted (b) data. (Bottom) Final image without (c) and with (d) the application of automatic muting. Without the mute, the image is unusable.



be maximal at the true subsurface point. However, in practice, due to limited frequency data, this ideal point is replaced by a high semblance region. The size of this region can be used to estimate the localization error margins that do not depend on the velocity model quality. Naturally, this procedure can also be repeated for different velocity models. In this example, we limited ourselves to bulk shifts (multiplying the entire model by a constant percentage) of the initial velocity model. Different semblance images built using bulk shifts of the initial velocity model are shown in Figure 7, demonstrating that when the correct velocity model is used, the diffraction is imaged at the correct location and its semblance value is maximal. In other words, for the synthetic case, a velocity analysis procedure, which is, in this case, a bulk shift scan, can be conducted using the semblance image itself instead of migrated gathers — the image yielding the highest coherence measure indicates the optimal migration velocity.

It is important to note why such an approach to the velocity model update was conducted. First, as shown in Figure 8, velocity models in our areas of interest consist of a strong vertical gradient with moderate lateral variations. Therefore, there are no clear layers that yield reflective/refractive events, and, therefore, layer-based approaches cannot be used. Moreover, given the scarcity of data, especially for the field data example shown later, updating such a complex model locally seems impossible due to the ill-posed nature of the inversion scheme. Therefore, we conclude that the scanning procedure aimed at calibrating a velocity model of which basic structure is determined from other methods is the optimal practical approach to the problem.

## REAL DATA EXAMPLE

A crosshole survey was conducted in the vicinity of a man-made cavity as shown in Figure 8. The lithology of the area is a mixture of sand and shales and occasionally sandstones, without clear boundaries between units. Due to overburden pressure and compaction,

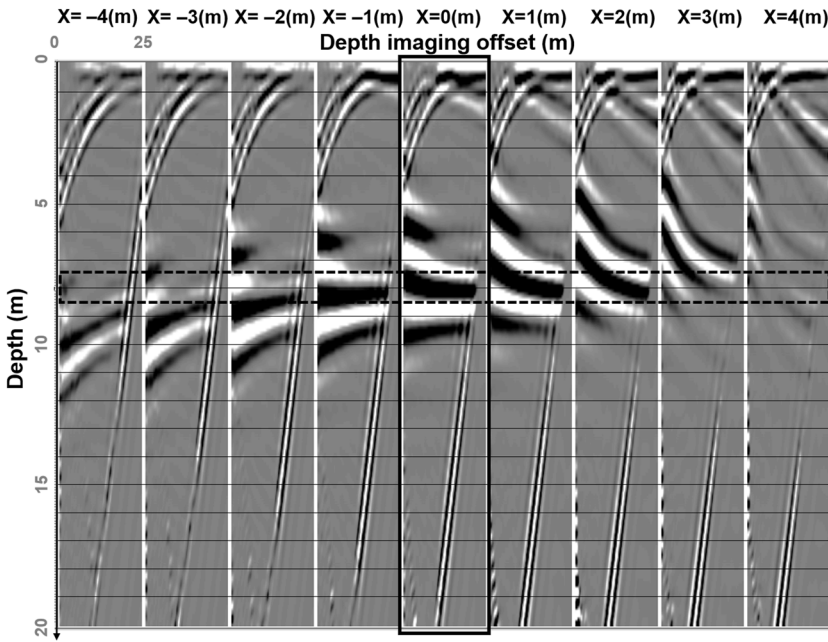


Figure 5. CIGs built at different locations using the correct velocity model. Here,  $x$  denotes the signed distance from the true void location along the  $x$ -axis. The correct depth is denoted by a dotted rectangle. At the correct location (solid rectangle), the event moveout is flat, whereas errors of 2 m and more yield bent moveouts of the same event.

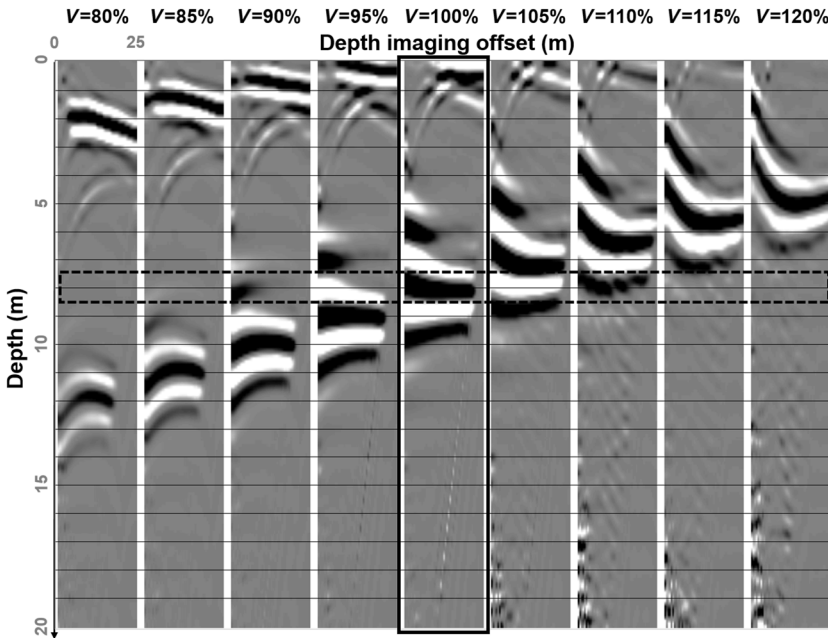


Figure 6. CIGs built at the correct diffraction point using different velocity models (bulk shifts). The correct depth is denoted by a dotted rectangle. At the correct velocity (solid rectangle), the event moveout is flat, whereas errors of 10% and more yield bent moveouts of the same event.

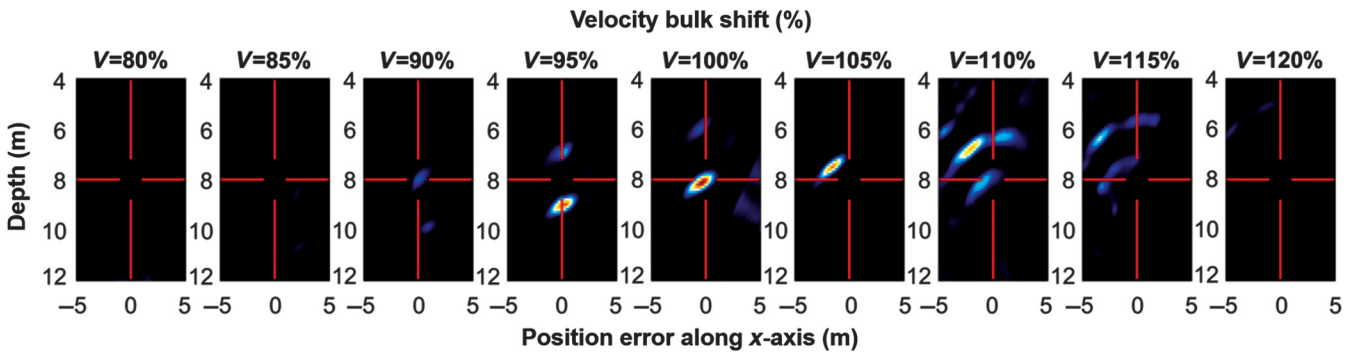


Figure 7. Semblance images built with different velocity bulk shifts. When the correct velocity is used, the semblance value is maximal and is at the correct spatial location (indicated by a cross).

the velocity increases with depth. At the surface level, we see very low velocities, representative of unconsolidated sediments. The survey cuts across the void, whose cross section was approximately  $1.80 \times 1$  m. The source polarity and the analyzed component of the 3C receiver were in the  $y$ -direction, to match the SH setup shown earlier. Sources and receivers were operated in cased boreholes. The downhole source we used was coupled to the casing at each shot depth using a clamp mechanism. Upon triggering, it released a uniaxial mechanical blow on the borehole casing. The orientation of the source could be controlled up to approximately  $10^\circ$ . For the receiver, we used a downhole 3C geophone with a clamping mechanism. For every shot depth, the receiver had to be moved and clamped to all possible receiver depths. Here again, the orientation was correct up to approximately  $10^\circ$ . We used a 10-shot stack on the field with a 1 kHz sampling frequency. The processing workflow consisted of combining the data to common-receiver gathers of the same component and band-pass filtering.

The direct S-wave arrivals were manually picked and used for a traveltimes tomography procedure, yielding the complex, laterally varying model shown in Figure 8. This model was also averaged to a regional 1D version, representing cases in which detailed knowledge of the velocity model will not be present. Alternatively,

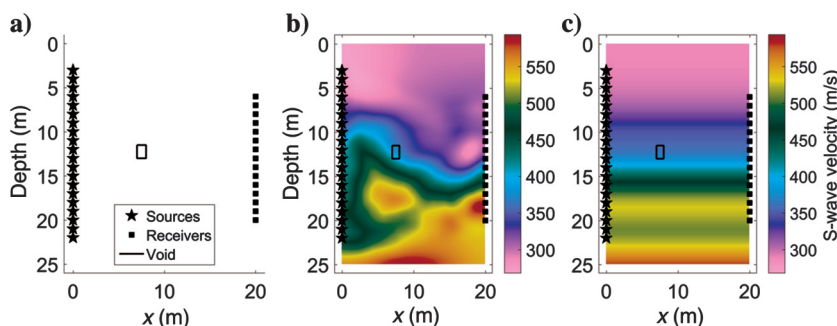


Figure 8. (a) Field setup, (b) S-wave tomography result, and (c) regional 1D model. Note the lateral variation of the model, superimposed on a strong vertical gradient.

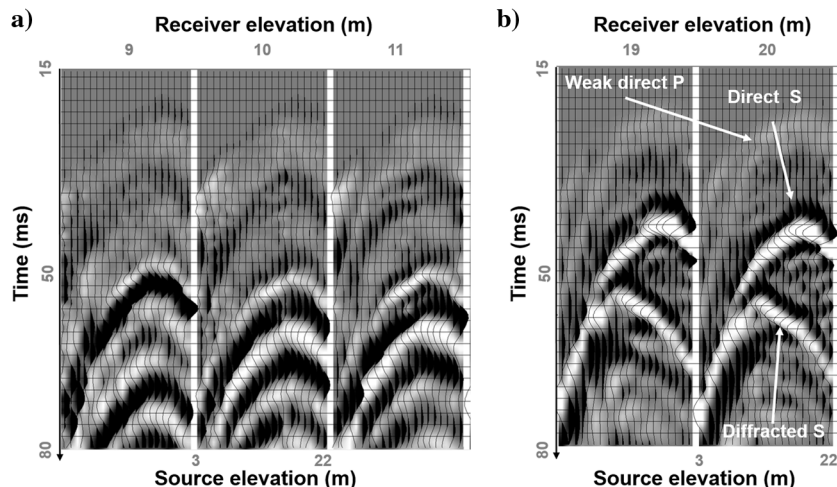


Figure 9. Crosshole data in common-receiver sorting ([a] close to void depth, [b] far from void depth) of the experimental setup, in common-receiver gathers. Here, P events are significantly weaker (though present) due to the acquisition setup and we see clear S first arrivals. The diffraction is clearly visible only in a few deep receivers.

one could use check-shot velocities, measured at the receivers' borehole, for the regional model. The data, organized in common-receiver gathers, are shown in Figure 9. Note that the diffraction is visible only in very few receivers. Therefore, we must first check the validity of applying the imaging procedure on such limited data. Let us go back to the synthetic data image, as shown in Figure 7. We will repeat this procedure using only two shot gathers in which the diffraction is clearly visible, at depths of 19 and 20 m (see Figure 3). The semblance image results of the entire data set versus the chosen scarce data set matching the field case are shown in Figure 10. This example shows that when such a small amount of data is used, the velocity analysis is not reliable. However, when the correct velocity model is used, the maximal semblance is obtained at the correct location. Therefore, we will not perform velocity analysis on the limited field data, and we will limit ourselves to correctly positioning the diffractive void.

It is important to mention that despite applying the automatic muting scheme we introduced, manual selection of the common-receiver records in which the diffraction is present is mandatory. As we see in this example, the diffraction's imprint is not always present in the data and in some records, for reasons inexplicable using modeling. The muting scheme is only capable of separating diffractions from direct arrivals — if the diffraction's imprint on the data is missing in records in which modeling predicts its clear existence, model-based muting would not prevent summation of noise into the image. Therefore, a combination of manual records selection and image-point dependent, model-based muting is necessary to image the diffraction. In our data set, only the few records compliant with those requirements were used for imaging.

In Figure 11, CIGs built from the selected field data, using the automatic muting scheme, at different locations are shown, using the full tomography and the regional model. When the full tomography model is used, the event moveout is flat at the correct spatial location. However, when the regional 1D model is used, the moveout is flat approximately 2 m to the left of the true location. This indicates the importance of using a detailed velocity model, easily extractable by direct wave picking and traveltimes tomography. If such a process cannot be conducted, errors in imaging will arise but gathers will still be usable. The result of applying a semblance measure on those gathers, effectively imaging the void, is shown in Figure 12. It shows that using a full tomography model yields a reliable image despite the small amount of data. However, when a regional model is used, a clear image is obtained but approximately 2 m to the left of the true location.

It is important to note that despite discrepancies in the  $x$  positioning of the void, by using both models, the depth of the flat moveout is correct. Due to this configuration, the analysis is more sensitive in depth positioning than lateral positioning, despite the larger complexity of

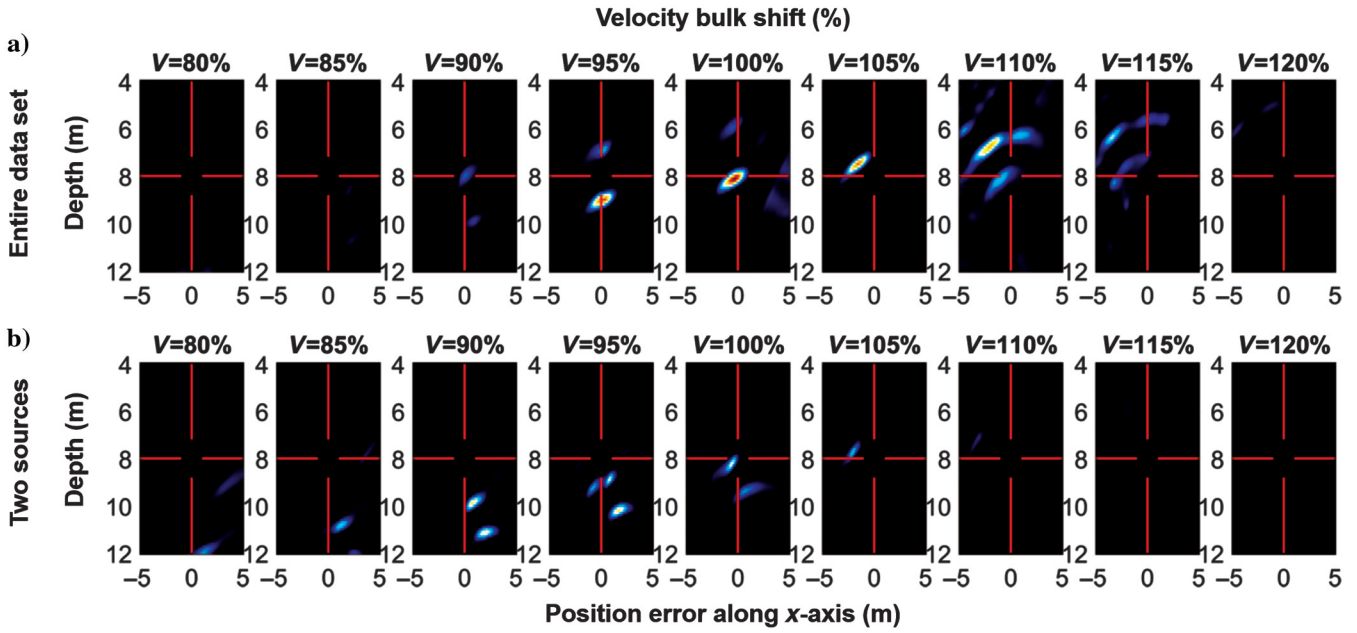


Figure 10. Semblance images built using different velocity bulk shifts using all synthetic data (a) and two chosen shots from it (b). Although a velocity analysis is possible when the entire data set is used, this is not the case for the scarce data. However, using the correct velocity model, the scarce data can be correctly imaged in space (the true location is indicated by a cross).

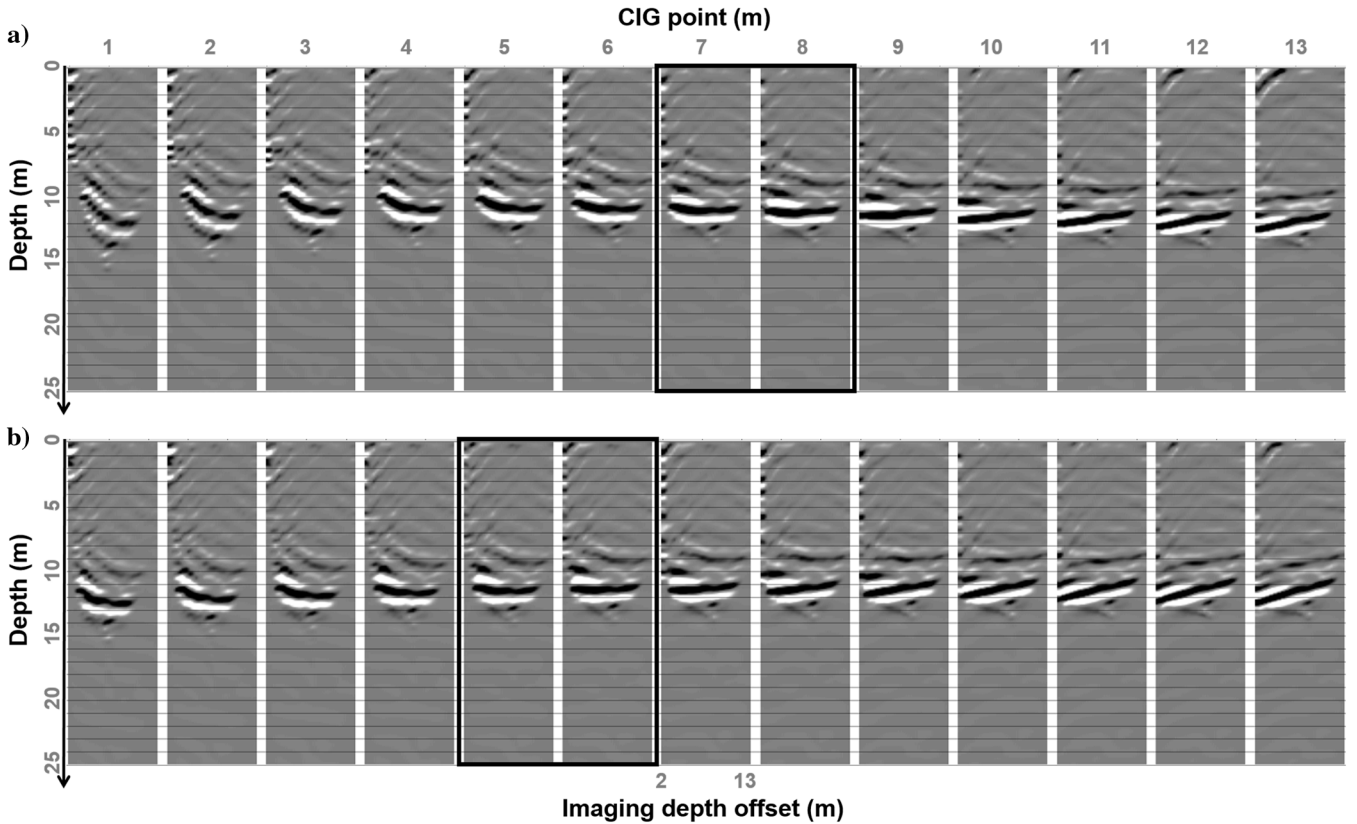


Figure 11. CIGs built at different imaging locations using the full tomography model (a) and regional model (b) seen in Figure 8. The true source location is at  $x = 7.5$  m and  $z = 11.5$  m. When the full tomography model is used, the event moveout is flat at the correct location and depth. However, when the regional model is used, an error of approximately 2 m in  $x$  arises despite maintaining the correct depth estimation.

the model in this dimension. As stated by [Eisner et al. \(2009\)](#) in their concluding remarks, the use of surface receivers is better at resolving  $x$ - $y$  uncertainty, whereas downhole receivers are better at resolving depth. In this example, we see yet another demonstration of those principles.

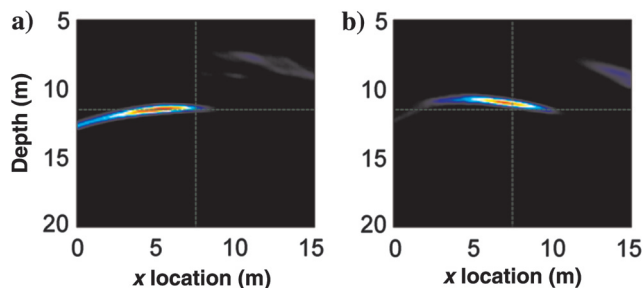


Figure 12. Semblance images built using the (a) regional model and (b) full tomography model. Although using the tomography model yields a precise image (the true location is indicated by a cross), the regional model induces an error of approximately 2 m in  $x$  — as seen in the gathers shown in Figure 11.

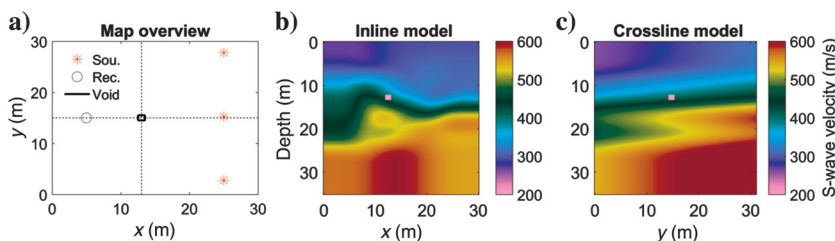


Figure 13. Simulative setup for the 3D test. (a) A map overview of the survey is shown. Sources are at depths of 20, 25, and 30 m, and receivers are spread between 3 and 30 m. The used velocity models along the dotted lines, intersecting with the void, are shown: (b) inline and (c) crossline. The  $V_P/V_S$  ratio is constant at 1.511, except inside the void where  $V_S = 0$  m/s,  $V_P = 340$  m/s.

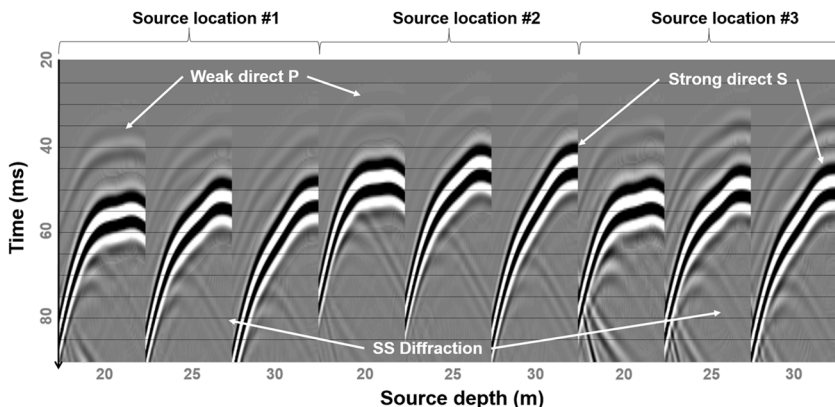


Figure 14. Synthetic data set computed using the setup from Figure 13, after polarity corrections. The direct S-waves are stronger than the P-waves due to the SH-optimized setup. The diffracted S-wave from the void is visible despite being much weaker than the direct arrivals. Note the effects of the velocity lateral variation — the direct waves' traveltimes from source location #3 are significantly shorter than those for source location #1 — despite both locations being at the same distance from the receivers.

### 3D SURVEYS

The use of surface receivers is, as stated in the “Introduction” section, problematic. However, using a single borehole is limited in terms of recovering the horizontal position of the void. Therefore, the natural solution is to use several boreholes, located in different spatial locations, to increase imaging precision. Because the model is more complex in its depth variation and we achieve a higher depth precision than a horizontal one, a relatively small amount of boreholes could prove sufficient.

We conducted a synthetic test, based on the extracted tomography model shown in Figure 8, to which we added a certain lateral variation in the out-of-plane dimension. The acquisition setup and used velocity model are shown in Figure 13. To represent scenarios as close as possible to our field example, we used a setup with very few sources but in which the direct arrivals are well-separated from the diffracted ones. Therefore, the source depths at each denoted location are at 20, 25, and 30 m, and receivers are spread between 3 and 30 m.

When sources are not at the same  $y$ -coordinate as the receivers, acquiring pure SH data (weak P-waves energy) becomes complex. As we have shown before (Figure 2), for 1D velocity models, pure SH data are obtained when source polarity and recording direction are perpendicular to the plane including sources and receivers. In this case, the velocity model has lateral variation so this will only be an approximation. Therefore, for this synthetic survey, we need to direct the sources according to their location in space. Accordingly, we need to extract the particle velocity measurement pointing to the same direction (e.g., for details of the procedure, see [MacBeth, 2002](#)). This can be achieved by rotating the source and receivers by the azimuth angle of the plane containing source and receivers, measured in reference to the Cartesian frame. After applying this correction, we obtain a relatively pure SH data set, shown in Figure 14. One can see that the SH-waves are dominant and that only an S-wave diffraction from the void is visible.

We will image the void using two different velocity models — the one used for simulation (shown in Figure 13) and its approximation, a 1D model extracted at the receiver's location. In Figure 15b, we show the different images obtained with those two velocity models. This proves the clear advantage of using the correct velocity model, correctly positioning the source with very high semblance values. In Figure 15a, we show the contribution of each separate shot location (locations shown in the left of Figure 13). This example shows that for a realistic imaging scenario in 3D, usage of multiazimuth acquisition is necessary because a single 2D survey yields a smeared image, even when using the true velocity model. For both cases, the depth at which the maximal coherency was obtained was at the true void position, as was the case for the field data example.

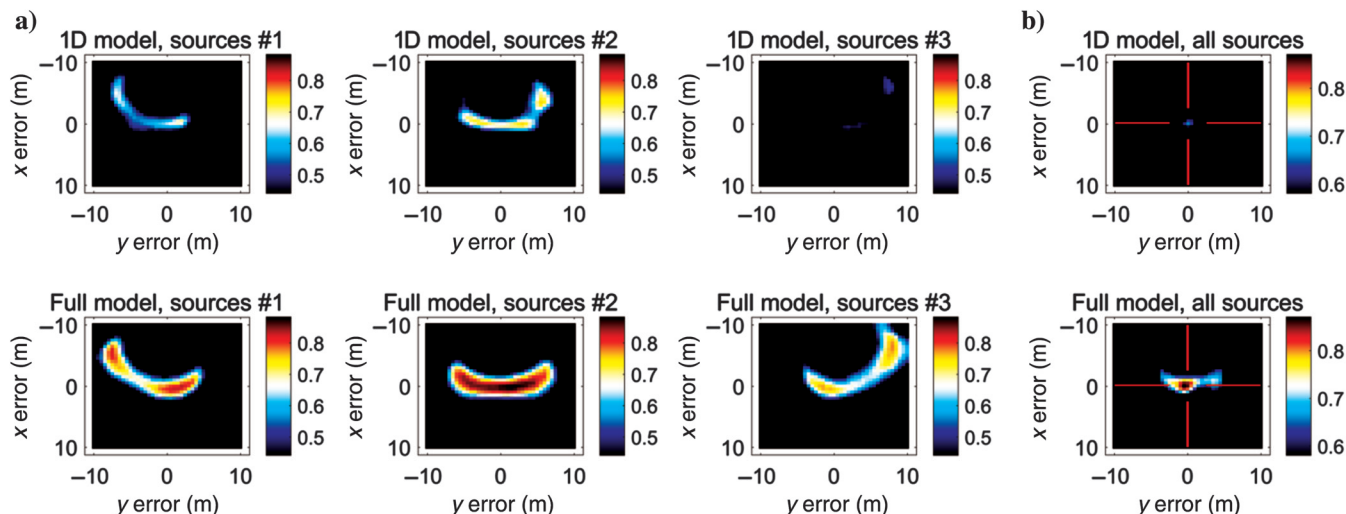


Figure 15. (a) Semblance images built using the 1D velocity model (top) and full velocity model (bottom) for separate shot locations. In both cases, using a single-source borehole location, the resulting image is smeared and no clear maximum occurs. (b) Semblance images built using all sources combined. Resulting coherency values are significantly higher for the correct velocity model, and their maximum is at the correct location (indicated by a cross). The combination of different azimuths is necessary for precise imaging.

## CONCLUSIONS

In this study, we showed the advantages of a multicomponent crosshole setup optimized for SH-waves recording for diffractive void detection and imaging. This setup has improved S/N, provided better resolution in depth, and helped in avoiding P/SV arrivals that might contaminate the diffractive part of the data. The SH crosshole survey is highly attractive for situations in which the vertical velocity gradient is significant because the separation between direct and diffracted SH phases can be observed in the acquired gathers. Overall, a significant part of the often challenging isolation of the diffractive part of the data is done at the acquisition stage, thus greatly simplifying the following imaging task. However, even in such a setup, diffracted events are separated only in some of the source-receiver pairs. Imaging of all the data might yield unusable results. The application of a model-based, image-point-dependent automatic muting, using traveltimes differences between the direct and diffracted events and calculated during the imaging process for each imaging point, mitigates that problem. Such a muting scheme is required because conventional diffraction extraction techniques were developed for separation from reflections and not from direct waves, thus, making them less suitable for the described setup.

Instead of directly imaging it, data can be first migrated into CIGs in the depth imaging offset domain. In this domain, velocity and location analysis can be conducted. Through synthetic and field examples, we show the CIGs' usefulness and sensitivity. However, in very low amounts of usable data, as presented by the field example, gathers do not have the required sensitivity for velocity analysis and only a location analysis is possible. Nonetheless, when a full traveltimes tomography model extracted from SH direct arrivals of the same crosshole data set is used, the imaged diffraction is at the correct location. When, instead, a regional 1D model is used, errors in  $x$  positioning arise despite yielding a single clear image. Since a crosshole survey is conducted anyhow, the tomography model building is a straightforward task.

In real-life scenarios, the use of multiazimuth acquisition is necessary. Without it, a single azimuthal survey yields a greatly

smeared image of the void. However, a relatively limited set of shot boreholes can prove sufficient given that various source depths are used. This acquisition setup requires proper orientation of the source and receivers to yield as pure (no P/SV) SH data as possible. When a 1D approximation of the varying velocity model is used, the resulting image has significantly lower coherency values. However, the use of multiple boreholes may also prove beneficial in building a detailed velocity model of the area, possibly through direct wave tomography.

## REFERENCES

- Auken, E., L. Pellerin, N. B. Christensen, and K. Sorensen, 2006, A survey of current trends in near-surface electrical and electromagnetic methods: *Geophysics*, **71**, no. 5, G249–G260, doi: [10.1190/1.2335575](https://doi.org/10.1190/1.2335575).
- Belfer, I., I. Bruner, S. Keydar, A. Kravtsov, and E. Landa, 1998, Detection of shallow objects using refracted and diffracted seismic waves: *Journal of Applied Geophysics*, **38**, 155–168, doi: [10.1016/S0926-9851\(97\)00025-6](https://doi.org/10.1016/S0926-9851(97)00025-6).
- Berkovitch, A., I. Belfer, Y. Hassin, and E. Landa, 2009, Diffraction imaging by multifocusing: *Geophysics*, **74**, no. 6, WCA75–WCA81, doi: [10.1190/1.3198210](https://doi.org/10.1190/1.3198210).
- Biondi, B., 2006, 3D seismic imaging: SEG.
- Cassidy, N. J., R. Eddies, and S. Dods, 2011, Void detection beneath reinforced concrete sections: The practical application of ground-penetrating radar and ultrasonic techniques: *Journal of Applied Geophysics*, **74**, 263–276, doi: [10.1016/j.jappgeo.2011.06.003](https://doi.org/10.1016/j.jappgeo.2011.06.003).
- Dasios, A., C. Mccann, T. R. Astin, D. M. Mccann, and P. Fenning, 1999, Seismic imaging of the shallow subsurface: Shear-wave case histories: *Geophysical Prospecting*, **47**, 565–591, doi: [10.1046/j.1365-2478.1999.00138.x](https://doi.org/10.1046/j.1365-2478.1999.00138.x).
- Dietrich, P., and J. Tronicke, 2009, Integrated analysis and interpretation of cross-hole P- and S-wave tomograms: A case study: *Near Surface Geophysics*, **7**, 101–109, doi: [10.3997/1873-0604.2008041](https://doi.org/10.3997/1873-0604.2008041).
- Eisner, L., P. M. Duncan, W. M. Heigl, and W. R. Keller, 2009, Uncertainties in passive seismic monitoring: *The Leading Edge*, **28**, 648–655, doi: [10.1190/1.3148403](https://doi.org/10.1190/1.3148403).
- Fomel, S., E. Landa, and M. T. Taner, 2007, Poststack velocity analysis by separation and imaging of seismic diffractions: *Geophysics*, **72**, no. 6, U89–U94, doi: [10.1190/1.2781533](https://doi.org/10.1190/1.2781533).
- Khaidukov, V., E. Landa, and T. J. Moser, 2004, Diffraction imaging by focusing-defocusing: An outlook on seismic superresolution: *Geophysics*, **69**, 1478–1490, doi: [10.1190/1.1836821](https://doi.org/10.1190/1.1836821).
- Korneev, V., 2009, Resonant seismic emission of subsurface objects: *Geophysics*, **74**, no. 2, T47–T53, doi: [10.1190/1.3068448](https://doi.org/10.1190/1.3068448).

- Landa, E., S. Fomel, and M. Reshef, 2008, Separation, imaging, and velocity analysis of seismic diffractions using migrated dip-angle gathers: 78th Annual International Meeting, SEG, Expanded Abstracts, 2176–2180.
- Landa, E., and S. Keydar, 1998, Seismic monitoring of diffraction images for detection of local heterogeneities: *Geophysics*, **63**, 1093–1100, doi: [10.1190/1.1444387](https://doi.org/10.1190/1.1444387).
- Lellouch, A., and M. Reshef, 2016, Usage of directional common image gathers for shallow seismic source localization: *Near Surface Geophysics*, **14**, 231–241, doi: [10.3997/1873-0604.2016012](https://doi.org/10.3997/1873-0604.2016012).
- MacBeth, C., 2002, Multi-component VSP analysis for applied seismic anisotropy: Pergamon.
- Manoogian, B. M. E., and V. W. Lee, 1996, Diffraction of SH-waves by subsurface inclusions of arbitrary shape: *Journal of Engineering Mechanics*, **122**, 123–129, doi: [10.1061/\(ASCE\)0733-9399\(1996\)122:2\(123\)](https://doi.org/10.1061/(ASCE)0733-9399(1996)122:2(123)).
- Paasche, H., M. Rumpf, J. Hausmann, T. Fechner, U. Werban, J. Tronicke, and P. Dietrich, 2013, Advances in acquisition and processing of near-surface seismic tomographic data for geotechnical site assessment: *First Break*, **31**, 59–65.
- Peterie, S. L., R. D. Miller, and D. W. Steeples, 2009, Diffraction imaging versus reflection processing for shallow void detection: 79th Annual International Meeting, SEG, Expanded Abstracts, 1421–1424, doi: [10.1190/1.3255115](https://doi.org/10.1190/1.3255115).
- Reshef, M., 2001, Some aspects of interval velocity analysis using 3D depth-migrated gathers: *Geophysics*, **66**, 261–266, doi: [10.1190/1.1444904](https://doi.org/10.1190/1.1444904).
- Rybakov, M., V. Goldshmidt, L. Fleischer, and Y. Rotstein, 2001, Cave detection and 4D monitoring: A microgravity case history near the dead sea: *The Leading Edge*, **20**, 896–900, doi: [10.1190/1.1487303](https://doi.org/10.1190/1.1487303).
- Shustak, M., N. Wechsler, A. Yurman, and M. Reshef, 2015, Comparison of surface vs. cross-hole seismic methods for void detection in the shallow sub-surface: 85th Annual International Meeting, SEG, Expanded Abstracts, 2286–2291, doi: [10.1190/segam2015-5900317.1](https://doi.org/10.1190/segam2015-5900317.1).
- Sloan, S. D., S. L. Peterie, R. D. Miller, J. Ivanov, J. R. McKenna, and S. W. Broadfoot, 2012, Tunnel detection using near-surface seismic methods: 82nd Annual International Meeting, SEG, Expanded Abstracts, doi: [10.1190/segam2012-1442.1](https://doi.org/10.1190/segam2012-1442.1).
- Walters, S. L., R. D. Miller, and J. Xia, 2007, Near surface tunnel detection using diffracted P-waves: A feasibility study: 77th Annual International Meeting, SEG, Expanded Abstracts, 1128–1132, doi: [10.1190/1.2792606](https://doi.org/10.1190/1.2792606).